Georgia Institute of Technology
a Unit of the University System of Georgia
Atlanta, Georgia 30332

SEMI-ANNUAL REPORT

ANALYSIS OF INTERLAMINAR FRACTURE IN COMPOSITES UNDER COMBINED LOADING

NASA GRANT **NAG-1-637**

GEORGIA TECH PROJECT **E-16-654**

PRINCIPAL INVESTIGATOR

ERIAN A. ARMANIOS

Overview

This report covers the research work performed under Grant NAG-1-637 for the period ending February 28, 1989. A detailed description of the fracture analysis of transverse crack tip delaminations is presented in the following sections. This work was performed during the first six months of the grant period and has been accepted for presentation at the 30th Structures, Structural Dynamics and Materials Conference (Mobile, Alabama, April 1989). The following sections are adapted from the aforementioned paper.

Abstract

Delamination is a predominant failure mode in continuous fiber reinforced laminated composite structures. One type of delamination is the transverse crack tip delamination which originates at the tip of transverse matrix cracks. An analytical model based on the sublaminate approach and fracture mechanics is developed in this paper to study the growth of such delaminations. Plane strain conditions are assumed and estimates are provided for the total strain energy release rate as well as the mode I and mode II contributions. The energy release rate estimates are used in combination with a simple failure law to predict critical delamination growth strains and stresses. These predictions are compared with experimental data on T300/934 Graphite Epoxy $[\pm 25/90_n]_s$ laminates in the range n=.5 to 8. A good agreement is demonstrated for the range of n where the experimental observations indicate transverse crack tip delamination to be the predominant failure mode.

Introduction

Fiber reinforced composites are now being used in a wide variety of engineering structures. The concept of directional strength and stiffness has been, for the most part, understood sufficiently to enable efficient load bearing designs. One of the current major issues in composite structures is the understanding and prediction of damage modes and failure mechanisms. A thorough knowledge of the failure mechanisms is bound to lead to the design of efficient and durable structures. Failures in these materials often initiate in the form of matrix cracks or delaminations. Matrix cracks refer to intralaminar failures whereas delaminations refer to interlaminar failures.

Matrix cracks usually occur within laminates where the fibers run at an angle to the primary load direction. Hence, such matrix cracks are also called transverse cracks. Based on the location and direction of growth, two distinct types of delamination can be discerned. These two types are called edge delamination and local or transverse crack tip delamination. Edge delaminations initiate at the load free edges of the laminate whereas local delaminations start from a transverse matrix crack. In many cases, both types occur concurrently with varying levels of interaction. It has been observed in simple tension tests of uniform rectangular cross section specimen (Edge Delamination tests) that delaminations initiate along the load free edges and propagate normal to the load direction. Transverse matrix cracks running parallel to the fibers have also been observed in off axis plies such as 90° plies. Such transverse cracks terminate where the ply orientation changes. Delaminations can also originate at the interfaces where transverse cracks terminate. These delaminations, called

transverse crack tip delaminations or local delaminations, grow normal to the transverse crack from which they originate. In the case of 90° plies, the growth direction is parallel to the load.

The growth process of edge delaminations and local delaminations is often modelled using a fracture mechanics approach leading to the calculation of a strain energy release rate. This is because the strain energy release rate can correlate delamination behavior from different loading conditions and can account for geometric dependencies. The strain energy release rate associated with a particular growth configuration is a measure of the driving force behind that failure mode. In combination with appropriate failure criteria, the strain energy release rate provides a means of predicting the failure loads of the structure.

Several methods are available in the literature for analyzing edge delaminations. These include finite element modelling[1-3], complex variable stress potential approach[4], simple classical laminate theory based technique[5] and higher order laminate theory including shear deformations[6]. Finite element models provide accurate solutions but involve intensive computational effort. Classical laminate theory (CLT) provides simple closed form solutions and is thus well suited for preliminary design evaluation. However, CLT provides only the total energy release rate, and thus, in a mixed mode situation, there is insufficient information to completely assess the delamination growth tendency. A higher order laminate theory including shear deformations has the ability to provide the individual contributions of the three fracture modes while retaining the simplicity of a closed form solution. A

shear deformation model is available for edge delamination and has been shown to agree well with finite element predictions[6].

Crossman and Wang[7] have tested T300/934 Graphite epoxy $[\pm 25/90_n]_s$ specimens in simple tension and reported a range of behavior including transverse cracking, edge delamination and local delamination. O'Brien[8] has presented classical laminate theory solutions for these specimen, demonstrating reasonable agreement in the case of edge delamination but with some discrepancies in the local delamination predictions. A finite element model combining edge and local delaminations has been proposed by Law[9]. His predictions, however, do not fully explain the dependency of the critical strain on the number of 90° plies.

In this paper, a shear deformation model is developed for the analysis of local delaminations originating from transverse cracks in 90° plies located in and around the specimen midplane. Plane strain conditions are assumed and thickness strain is neglected. Delaminations are assumed to grow from both ends of the transverse crack tip. The transverse crack is treated as a free boundary and the delamination is considered to be the crack whose growth behavior is to be modelled. The sublaminate approach[10,11] is used to model different regions of the specimen. The resulting boundary value problem is solved to obtain the interlaminar stresses, total strain energy release rate and energy release rate components. Critical local delamination growth loads are predicted for $[\pm 25/90_n]_s$ specimens.

Analytical Model

The formulation is based on the sublaminate approach detailed in Ref. 10. A longitudinal section illustrating the geometry of a generic

configuration is shown in fig. 1. The central region is assumed to be made of 90° plies with an isolated transverse crack in the middle. Delaminations are assumed to grow from both ends of the transverse crack, and towards both ends as shown. From symmetry considerations, only one quarter of the configuration is modelled. The modelled portion is divided into four sublaminates as shown in fig. 2. The top surface (sublaminates 1 and 4) is stress free. In order to simplify the analysis, plane strain conditions are assumed and the thickness strain (ε_z) is set to zero. The consequence of this, combined with the fact that the w displacement is zero along the center line, is that w is zero in sublaminates 1, 2 and 3. Also, this approximation does not allow for the enforcement of boundary conditions on the shear stress resultants, leading to incorrect estimates of the interlaminar normal stresses. The interlaminar shear stresses, however, are not affected by this assumption[6,10]. These assumptions lead to considerable simplifications in the analysis. In spite of the simplifications, reliable energy release rate components can be estimated based on the interlaminar shear stress distributions[6,10].

A generic sublaminate is shown in fig. 3 along with the notations and sign conventions. The peel and interlaminar shear stresses are denoted by P and T, respectively, with t and b subscripts for the top and bottom surfaces, respectively. The axial stress resultant, shear stress resultant and bending moment resultant are denoted by N, Q and M, respectively. A summary of the governing equations is presented in the following paragraphs for convenience. These equations are derived for a generic sublaminate using the principle of virtual work in Ref.12.

The x and z displacements within the sublaminate are assumed to be of the form

$$u(x,z) = U(x)+z\beta(z) \tag{1}$$

$$w(x,z) = W(x) \tag{2}$$

Here U represents the axial midplane stretching and W is the transverse displacement. The shear deformation is recognized through the rotation β. The origin of the coordinate axes for the sublaminates is taken at the delamination tip as shown in fig. 4. The equilibrium equations take the form

$$N_{,x}+T_t-T_b = 0 \tag{3}$$

$$Q_{,x}+P_t-P_b = 0 \tag{4}$$

$$M_{,x}-Q+\frac{h}{2}(T_t+T_b) = 0 \tag{5}$$

where h is the thickness of the sublaminate. The constitutive relations in terms of the force and moment resultants are

$$N = A_{11}U_{,x}+B_{11}\beta_{,x} \tag{6}$$

$$Q = A_{55}(\beta+W_{,x}) \tag{7}$$

$$M = B_{11}U_{,x}+D_{11}\beta_{,x} \tag{8}$$

where A_{ij}, B_{ij} and D_{ij} are the classical laminate theory axial, coupling and bending stiffnesses, respectively. The boundary variables to be prescribed at the sublaminate edges are

N or U

M or β

Q or W

Additionally, at the interfaces between sublaminates, reciprocal traction and displacement matching boundary conditions have to specified.

Solution Procedure

A detailed solution is provided in the Appendix. A summary is provided in this section for convenience. The variables are subscripted to indicate the sublaminate in which they occur. The solutions in sublaminates 1 and 2 are coupled by the reciprocal interlaminar stresses denoted T_1 and P_1 and by displacement continuity at the common interface. Assuming exponential solutions for the axial force and bending moment resultants leads to an eigenvalue problem involving the exponential parameter s. The eigenvalues turn out to be 0 and two nonzero values (say s_1 and s_2) occurring in positive and negative pairs. Since the response decays from the delamination (crack) tip, only the exponentially decaying terms are considered in the solutions.

The following boundary conditions from the ends of the modelled region are enforced.

$$N_2(0) = 0 \tag{9}$$

$$Q_4(a) = 0 \tag{10}$$

$$\beta_4(a) = 0 \tag{11}$$

$$N_1+N_2 = \text{Applied Load} \tag{12}$$

Further, the following displacement matching conditions are applied.

$$u_1\left(x,-\frac{h_1}{2}\right) = u_2\left(x,\frac{h_2}{2}\right) \tag{13}$$

$$U_1(0) = U_4(0) \tag{14}$$

$$U_2(0) = U_3(0) \tag{15}$$

$$\beta_1(0) = \beta_4(0) \tag{16}$$

It should be noted that a β_2 and β_3 matching condition cannot be applied at this level of modeling since it would amount to specifying both W and Q[6,12]. Consequently, there is a displacement discontinuity

at the delamination tip. The effect of this will be discussed subsequently. To eliminate rigid body displacements, U_1 is set to zero at the left end. The following solutions can then be obtained for the resultants in sublaminates 1 and 2.

$$N_1 = a_1 e^{s_1 x} + a_2 e^{s_2 x} + \varepsilon A_{11(1)} \tag{17}$$

$$N_2 = -a_1 e^{s_1 x} - a_2 e^{s_2 x} + \varepsilon A_{11(2)} \tag{18}$$

$$M_1 = a_1 k_1 e^{s_1 x} + a_2 k_2 e^{s_2 x} \tag{19}$$

$$M_2 = a_1 k_3 e^{s_1 x} + a_2 k_4 e^{s_2 x} \tag{20}$$

The interlaminar shear and peel stresses between sublaminates 1 and 2 can be obtained from equilibrium as

$$T_1 = a_1 s_1 e^{s_1 x} + a_2 s_2 e^{s_2 x} \tag{21}$$

$$P_1 = \left(k_1 + \frac{h_1}{2}\right)\left(a_1 s_1^2 e^{s_1 x}\right) + \left(k_2 + \frac{h_1}{2}\right)\left(a_2 s_2^2 e^{s_2 x}\right) \tag{22}$$

In the above solutions, the k_i parameters are dependent on the eigenvalues and the stiffness of sublaminates 1 and 2, the a_j parameters depend on the k_i parameters and the crack length a, and ε is defined as

$$\varepsilon = \frac{P}{2b} \frac{1}{A_{11(1)} + A_{11(2)}} \tag{23}$$

where P is the uniform axial force applied on the specimen and b is the specimen width. Expressions for the eigenvalues and the a_j and k_i parameters are provided in the Appendix.

Proceeding on to sublaminates 3 and 4, the following solutions can be written.

$$N_3 = 0 \tag{24}$$

$$M_3 = \varphi_1 \sinh(\omega_3 x) + \varphi_2 \cosh(\omega_3 x) \tag{25}$$

where

$$\varphi_2 = a_1 k_3 + a_2 k_4, \tag{26}$$

$$\varphi_1 = -\varphi_2 \coth(\omega_3 a), \tag{27}$$

and

$$\omega_3 = \sqrt{\frac{A_{55(2)}}{D_{11(2)}}} \tag{28}$$

$$N_4 = \varepsilon \left(A_{11(1)}+A_{11(2)}\right) \tag{29}$$

$$M_4 = a_1 k_1 + a_2 k_2 \tag{30}$$

The corresponding displacement solutions are provided in the Appendix. The compliance of the specimen can be evaluated as

$$C = 2\frac{U_4(a)}{P} \tag{31}$$

The total energy release rate, G_T, per crack is then given by

$$G_T = \frac{P^2}{2b}\frac{dC}{da} \tag{32}$$

Use of the previously described solutions leads to the following expression.

$$G_T = \frac{P^2}{2b^2}\left(\frac{1}{A_{11(1)}} - \frac{1}{A_{11(1)}+A_{11(2)}} + I_1 - I_2\right) \tag{33}$$

where the quantities I_1 and I_2 contain exponential terms dependent on the delamination length. Using the virtual crack closure technique, from the relative displacements in the cracked portion and the interlaminar stresses ahead of the crack tip, the mode I and mode II energy release rate contributions can be obtained. The mode III energy release rate is zero from the assumption of plane strain. The mode II energy release rate is given by

$$G_{II} = \lim_{\delta \to 0} \frac{1}{2\delta} \int_0^{\delta} T_1(x-\delta)\Delta u(x)dx \tag{34}$$

where δ is the virtual crack step size. The result of the limiting process is zero if there is no singularity in the stress field[10]. So, the limit is usually taken as the crack step size d tends to a small value, say Δ, based on the decay length or the length required to capture the

essential features of the stress and displacement fields near the crack tip. The decay length is dependent on the eigen values s_1 and s_2. In this study, the value of Δ has been set to

$$\Delta = \frac{1}{4}\left(\frac{1}{s_1} + \frac{1}{s_2}\right) \tag{35}$$

since it reasonably fulfills the criterion given above. In a similar fashion, the mode I energy release rate can be obtained based on the normal stress (P) and the w displacements near the crack front. The normal (peel) stress estimate is inaccurate due to the absence of thickness strain. Hence, an alternate approach was used to estimate G_I, the mode I energy release rate. The total energy release rate for this problem is made up entirely of G_I and G_{II} (G_{III}=0). From an estimate of G_T and G_{II}, an estimate for G_I can be obtained simply as

$$G_I = G_T - G_{II} \tag{36}$$

The critical load for a given specimen can then be evaluated based on an appropriate fracture law. This is illustrated in the following section.

Results and Discussion

The solutions derived in the previous section have been used to model the behavior of $[\pm 25/90_n]_s$ T300/934 Graphite Epoxy specimen for n values of .5,1,2,3,4,6,and 8. These correspond to the specimen tested by Crossman and Wang[7]. The specimen width and length were fixed at .0381m and .015m, respectively, as in the tests and the applied uniform axial stress was 100MPa. The solutions were generated using a simple computer program based on the closed form expressions for the interlaminar stress and energy release rates.

An example of the total energy release rate variation with the crack length is presented in fig. 5. The asymptotic value of G_T is denoted by G_{T0} in the figure. It can be observed that after a certain crack length, the G_T is independent of the crack length. On the basis of curves like the one shown in fig. 5, the crack length was fixed at 10 ply thicknesses for the remainder of the study. The dependence of the mode II contribution of the energy release rate on crack length (a) is depicted in fig. 6. Typical interlaminar shear and normal stress profiles are presented in figs. 7 and 8, respectively. The corresponding energy release rates have also been calculated and are presented in Table I and fig. 9.

In order to evaluate the critical loads, an appropriate mixed mode fracture law has to be applied, based on the calculated energy release components. Since the calculated mode split shows only a small variation with n, the simple Griffith criterion $G_T=G_{Tc}$ has been used to scale the stresses to obtain the critical delamination growth stress (σ_c) and strain (ε_c) values. The critical energy release rate G_{Tc} was chosen as 415 J/m^2 to obtain the critical stresses and strains listed in Table I. This value of G_{Tc} is larger than G_{Ic} to account for the presence of mode II and the fact that for the material system under consideration, G_{IIc} is about four times G_{Ic}. The critical strains are plotted against n, the number of 90° plies in fig. 10. The experimental results of Ref. 7 and the predictions of Refs. 8 and 9 are also presented in the figure for comparison. The predictions of the model developed in this paper are represented by the solid line while the experimental results are shown as filled squares. The classical laminate theory and finite element critical strain predictions of Refs. 8 and 9

are represented by triangles with a connecting line and a dotted line respectively. The CLT based model agrees well with the shear deformation model in terms of the total energy release rate. However, the CLT based model does not provide information on the mode split and thus, the value of $G_c(\approx G_{Ic})$ used leads to bias in the predictions.

In the experiments, the local delamination phenomenon was observed as the predominant failure mode only for the n=4, 6 and 8 specimens. The shear deformation model presented in this paper provides good agreement with the experimental data in this range. For n<4, edge delamination either in the mid plane or in the 25/90 interface was observed in the tests. Hence, the predictions of the local delamination models in this region are not of consequence as long as they do not predict critical loads lower than those predicted by edge delamination models. Thus, it can be seen that the shear deformation model predicts the observed behavior with reasonable accuracy and can be used in conjunction with an appropriate edge delamination model to predict critical loads accurately for the complete range of n values. The edge delamination model presented in Refs. 6 and 12 can be used for this purpose. However, a separate model is required to account for the midplane (Mode I) edge delamination behavior. The development of such a model is described in Ref. 13.

Conclusions

A shear deformation model has been developed to analyze local delaminations growing from transverse cracks in 90° plies located around the mid plane of symmetric laminates. The total energy release rate calculations yield the same results as in the case of CLT based models. The predictions of the shear deformation model agree

reasonably with critical strain experimental data from $[\pm 25/90_n]_s$ T300/934 Graphite Epoxy laminates. The predicted behavior is such that, in combination with an edge delamination model, the critical loads can be predicted accurately in the range of n from .5 to 8.

Acknowledgements

The authors gratefully acknowledge the financial support provided by NASA under grant NAG-1-637 for performing the research reported in this paper. The authors also wish to thank Mr. A. Badir for help in verifying the analytical model.

References

[1] Wilkins, D.J., Eisemann, J.R., Camin, R.A., Margolis, W.S. and Benson, R.A., "Characterizing Delamination Growth in Graphite-Epoxy," in Damage in Composite Materials, ASTM STP 775, K.L. Reifsnider, Ed., pp. 168-183 (1982).

[2] O'Brien, T.K., "Mixed-Mode Strain Energy Release Rate Effects on Edge Delamination of Composites," in Effects of Defects in Composite Materials, ASTM STP 836, pp. 125-142 (1984).

[3] Wang, S.S. and Choi, I., "The Mechanics of Delamination in Fiber Reinforced Composite Materials. Part II - Delamination Behavior and Fracture Mechanics Parameters," NASA CR-172270 (1983).

[4] Wang, S.S., "Edge Delamination in Angle Ply Composite Laminates," Proceedings of the 22nd AIAA/ASME/ASCE/AHS Structures, Structural Dynamics and Materials Conference, Atlanta, Georgia, 6-8 April, 1981, pp. 473-484.

[5] O'Brien, T.K., "Characterization of Delamination Onset and Growth in a Composite Laminate," in Damage in Composite

Materials, ASTM STP 775, K.L. Reifsnider, Ed., pp. 140-167 (1982).

[6] Armanios, E.A., and Rehfield, L.W., "Interlaminar Analysis of Laminated Composites using a Sublaminate Approach," Proceedings of the 27th AIAA/ASME/ASCE/AHS Structures, Structural Dynamics and Materials Conference, San Antonio, Texas, 19-21 May, 1986, Part 1, pp. 442-452. AIAA Paper 86-0969CP.

[7] Crossman, F.W., and Wang, A.S.D.,"The Dependence of Transverse Cracking and Delamination on Ply Thickness in Graphite/Epoxy Laminates," in Damage in Composite Materials, ASTM STP 775, K.L. Reifsnider, Ed., pp. 118-139 (1982).

[8] O'Brien, T.K., "Analysis of Local Delaminations and Their Influence on Composite Laminate Behavior," in Delamination and Debonding of Materials, ASTM STP 876, Johnson, W.S., Ed., pp. 282-297 (1985).

[9] Law, G.E., "A Mixed Mode Fracture Analysis of $(\pm 25/90_n)_s$ Graphite/Epoxy Composite Laminates," in Effects of Defects in Composite Materials, ASTM STP 836, pp. 143-160 (1984).

[10] Armanios, E.A., "New Methods of Sublaminate Analysis for Composite Structures and Applications to Fracture Processes," Ph.D. Thesis, Georgia Institute of Technology (1984).

[11] Armanios, E.A., Rehfield, L.W., and Reddy, A.D., "Design Analysis and Testing for Mixed-Mode and Mode II Interlaminar Fracture of Composites," in Composite Materials: Testing and Design (Seventh Conference), ASTM STP 893, J.M.Whitney, Ed., pp. 232-255 (1986).

[12] Armanios, E.A., and Rehfield, L.W., "Sublaminate Analysis of Interlaminar Fracture in Composites: Part I - Analytical Model," submitted for publication in the Journal of Composites Technology and Research (July, 1988).

[13] Armanios, E.A., Badir, A., and Sriram, P., "Sublaminate Analysis of Mode I Edge Delamination in Laminated Composites," 30th AIAA/ASME/ASCE/AHS Structures, Structural Dynamics and Materials Conference, Mobile, Alabama (April 1989).

Appendix

Sublaminate Analysis for Local Delaminations

A generic sublaminate is shown in fig. 3 along with the notations and sign conventions. The interlaminar normal (peel) and shear stresses are denoted by P and T respectively with the t and b subscripts for the top and bottom surfaces respectively. The axial force resultant, shear force resultant and bending moment resultant are denoted by N, Q and M respectively. Plane strain conditions are assumed to prevail in the x-z plane and the thickness strain ε_{zz} is neglected. These assumptions lead to considerable simplification in the analysis. The displacements in the x and z directions are assumed to be of the form

$$u = U(x)+zb(x) \tag{A.1}$$

$$w = W(x) \tag{A.2}$$

Here U represents the axial stretching and W is the transverse (thickness direction) displacement. This formulation recognizes shear deformation through the rotation β. The equilibrium equations take the form

$$N_{,x}+T_t-T_b = 0 \tag{A.3}$$

$$Q_{,x}+P_t-P_b = 0 \tag{A.4}$$

$$M_{,x}-Q+\frac{h}{2}(T_t+T_b) = 0 \tag{A.5}$$

where h is the thickness of the sublaminate. The constitutive equations in terms of the force and moment resultants are

$$N = A_{11}U_{,x}+B_{11}\beta_{,x} \tag{A.6}$$

$$Q = A_{55}(\beta+W_{,x}) \tag{A.7}$$

$$M = B_{11}U_{,x}+D_{11}\beta_{,x} \tag{A.8}$$

where A,B and D are the classical laminate theory axial, coupling and bending stiffnesses defined in the customary manner as

$$(A_{ij},B_{ij},D_{ij}) = \int_{-h/2}^{h/2} C_{ij}(1,z,z^2)dz$$

Here, the C_{ij}s are the material moduli. For the case of plane strain in the x-z plane, the Cs are defined as follows.

$$\begin{Bmatrix}\sigma_{xx}\\ \sigma_{zz}\\ \tau_{xz}\end{Bmatrix} = \begin{bmatrix}C_{11} & C_{13} & 0\\ C_{13} & C_{22} & 0\\ 0 & 0 & C_{55}\end{bmatrix}\begin{Bmatrix}\varepsilon_{xx}\\ \varepsilon_{zz}\\ \gamma_{xz}\end{Bmatrix} \tag{A.9}$$

The boundary quantities to be prescribed at the sublaminate edges are

N or U

M or β

Q or W

Further, at the interfaces between sublaminates, reciprocity of tractions and continuity of displacements have to be enforced.

The four sublaminates along with the loads acting on each are shown in fig. 4. Setting P_1 and T_1 as shown automatically satisfies the traction matching boundary condition at the 1-2 interface. From symmetry, we get w=0 and zero shear stress along the bottom faces of

sublaminates 2 and 3. This leads to w=0 in sublaminates 1, 2 and 3. Thus, W has been prescribed in these sublaminates and the vertical shear force resultant Q cannot be prescribed on these sublaminates. Consequently, the calculated peel stress distribution will not be correct. In addition, at the 2-3 interface, the βs cannot be matched, since in these sublaminates, specifying β is equivalent to specifying Q (through Eq. A.7). Inspite of these simplifications, reliable energy release rate components can be estimated based on the interlaminar shear stress distributions. The mode I contribution can then be evaluated using the total energy release rate, which is not affected significantly by these simplifications.

For the $(\pm 25/90_n)_s$ laminates under consideration, B_{11} is zero in all the four sublaminates. For sublaminates 1 and 2, the equilibrium equations and constitutive relationships can be written as

$$N_{1,x} - T_1 = 0 \tag{A.10}$$

$$N_{2,x} + T_1 = 0 \tag{A.11}$$

$$Q_{1,x} - P_1 = 0 \tag{A.12}$$

$$Q_{2,x} + P_1 - P_2 = 0 \tag{A.13}$$

$$M_{1,x} + \frac{h_1}{2} T_1 - Q_1 = 0 \tag{A.14}$$

$$M_{2,x} + \frac{h_2}{2} T_1 - Q_2 = 0 \tag{A.15}$$

$$N_1 = A_{11(1)} U_{1,x} \tag{A.16}$$

$$N_2 = A_{11(2)} U_{2,x} \tag{A.17}$$

$$Q_1 = A_{55(1)} \beta_1 \tag{A.18}$$

$$Q_2 = A_{55(2)} \beta_2 \tag{A.19}$$

$$M_1 = D_{11(1)} \beta_{1,x} \tag{A.20}$$

$$M_2 = D_{11(2)} \beta_{2,x} \tag{A.21}$$

The subscripts in parentheses refer to the sublaminates to which the stiffness coefficients correspond. Eqs. A.14, A.15 and A.12 can be rewritten in a modified form as

$$M_{1,x} + \frac{h_1}{2} N_{1,x} = A_{55(1)}\beta_1 \tag{A.22}$$

$$M_{2,x} - \frac{h_2}{2} N_{2,x} = A_{55(2)}\beta_2 \tag{A.23}$$

$$P_1 = Q_{1,x}$$
$$= M_{1,xx} + \frac{h_1}{2} T_{1,x} \tag{A.24}$$

Matching the u displacement along the 1-2 interface implies

$$u_1\left(x,-\frac{h_1}{2}\right) = u_2\left(x,\frac{h_2}{2}\right)$$

or

$$U_1 - \frac{h_1}{2} b_1 = U_2 + \frac{h_2}{2} b_2 \tag{A.25}$$

Combining the equations to eliminate the displacement and interlaminar stress terms leads to the following system of homogeneous coupled ordinary differential equations.

$$N_{1,x}+N_{2,x} = 0 \tag{A.26}$$

$$M_{1,xx}+\frac{h_1}{2} N_{1,xx} - \frac{A_{55(1)}}{D_{11(1)}} M_1 = 0 \tag{A.27}$$

$$M_{2,xx}-\frac{h_2}{2} N_{2,xx} - \frac{A_{55(2)}}{D_{11(2)}} M_2 = 0 \tag{A.28}$$

$$\frac{N_1}{A_{11(1)}} - \frac{h_1 M_1}{2D_{11(1)}} - \frac{N_2}{A_{11(2)}} - \frac{h_2 M_2}{2D_{11(2)}} = 0 \tag{A.29}$$

The solution is assumed of the form

$$\begin{Bmatrix} N_1 \\ N_2 \\ M_1 \\ M_2 \end{Bmatrix} = \begin{Bmatrix} A_1 \\ A_2 \\ A_3 \\ A_4 \end{Bmatrix} e^{sx} \tag{A.30}$$

Substitution of this solution into Eqs. A.26-A.29 leads to an eigenvalue problem with the following characteristic equation.

$$s[B_1 s^4 + B_2 s^2 + B_3] = 0 \tag{A.31}$$

where the B's involve the stiffness and thickness parameters A, D and h. For the material system and ply stacking sequence considered, $B_2^2 > 4B_1B_3$. Hence, the roots can be written as

$$s = 0, \pm\sqrt{\frac{-B_2 \pm \sqrt{B_2^2 - 4B_1B_3}}{2B_1}} \tag{A.32}$$

Only the zero and positive roots of eq. A.32 are considered as they give solutions decaying exponentially from the crack tip. Then, the axial force and moment resultants can be written as

$$N_1 = a_1 e^{s_1 x} + a_2 e^{s_2 x} + a_1 \tag{A.33}$$

$$N_2 = -a_1 e^{s_1 x} - a_2 e^{s_2 x} + a_2 \tag{A.34}$$

$$M_1 = a_1 k_1 e^{s_1 x} + a_2 k_2 e^{s_2 x} \tag{A.35}$$

$$M_2 = a_1 k_3 e^{s_1 x} + a_2 k_4 e^{s_2 x} \tag{A.36}$$

The k parameters in the above solutions involve the eigenvalues and the stiffness coefficients (A,D). For example, we have the definition for k_1 as

$$k_1 = \frac{\frac{h_1}{2} s_1^2}{\frac{A_{55(1)}}{D_{11(1)}} - s_1^2} \tag{A.37}$$

Using the equilibrium Eqs. A.10, A.12 and A.14 along with the applied axial force P and specimen width b, the axial force resultants and interlaminar stresses can be written as

$$N_1 = a_1 e^{s_1 x} + a_2 e^{s_2 x} + \frac{P}{2b} \frac{A_{11(1)}}{A_{11(1)} + A_{11(2)}} \tag{A.38}$$

$$N_2 = -a_1 e^{s_1 x} - a_2 e^{s_2 x} + \frac{P}{2b} \frac{A_{11(2)}}{A_{11(1)} + A_{11(2)}} \tag{A.39}$$

$$T_1 = N_{1,x} = a_1 s_1 e^{s_1 x} + a_2 s_2 e^{s_2 x} \tag{A.40}$$

$$P_1 = M_{1,xx} + \frac{h_1}{2} T_{1,x}$$

$$= \left(k_1+\frac{h_1}{2}\right)a_1 s_1^2 e^{s_1 x}+\left(k_2+\frac{h_1}{2}\right)a_2 s_2^2 e^{s_2 x} \qquad (A.41)$$

The constitutive equations are used to write down the displacement solutions. The arbitrary constants associated with the displacements and rotations are determined from the matching conditions between sublaminates 1 and 2 and the end conditions. Proceeding to sublaminate 3, the governing equations are

$$N_{3,x} = 0 \qquad (A.42)$$

$$Q_{3,x} + P_3 = 0 \qquad (A.43)$$

$$M_{3,x} - Q_3 = 0 \qquad (A.44)$$

$$N_3 = A_{11(2)} U_{3,x} \qquad (A.45)$$

$$Q_3 = A_{55(2)} \beta_3 \qquad (A.46)$$

$$M_3 = D_{11(2)}\, \beta_{3,x} \qquad (A.47)$$

Matching U at the 2-3 interface and applying the boundary condition at the free end, $N_3(a) = 0$, gives

$$N_3 = 0 \qquad (A.48)$$

$$U_3 = U_2(0) = -\frac{a_1}{s_1 A_{11(2)}} - \frac{a_2}{s_2 A_{11(2)}} + a_3 \qquad (A.49)$$

In order to solve for the bending moment, Eqs. A.44, A.46 and A.47 are combined to yield

$$M_3 = \varphi_1 \sinh \omega_3 x + \varphi_2 \cosh \omega_3 x \qquad (A.50)$$

where ω_3 is defined by

$$\omega_3 = \sqrt{\frac{A_{55(2)}}{D_{11(2)}}} \qquad (A.51)$$

Since the β matching conditon cannot be used at the 2-3 interface, the (remaining) boundary conditions are

$$M_3(a) = 0 \qquad (A.52)$$

$$M_3(0) = M_2(0) \qquad (A.53)$$

The φs can be solved using the boundary conditions A.52 and A.53 as

$$\varphi_2 = a_1 k_3 + a_2 k_4 \tag{A.54}$$

$$\varphi_1 = -\varphi_2 \coth \omega_3 a \tag{A.55}$$

The solution for sublaminate 3 can be completed by writing the expressions for Q_3, β_3 and P_3 based on the M_3 solution.

The equilibrium equations for sublaminate 4 are

$$N_{4,x} = 0 \tag{A.56}$$

$$Q_{4,x} = 0 \tag{A.57}$$

$$M_{4,x} - Q_4 = 0 \tag{A.58}$$

The constitutive relations take the form

$$N_4 = A_{11(1)} U_{4,x} \tag{A.59}$$

$$Q_4 = A_{55(1)} (\beta_4 + W_{4,x}) \tag{A.60}$$

$$M_4 = D_{11(1)} \beta_{4,x} \tag{A.61}$$

Using Eq. A.56 with the boundary condition $N_4(a) = \frac{P}{2b}$ yields

$$N_4 = \frac{P}{2b} \tag{A.62}$$

Similarly, using Eq. A.57 with $Q_4(a)=0$ results in

$$Q_4 = 0 \tag{A.63}$$

Matching M_1 and M_4 at the 1-4 interface and using Eq. A.58 gives

$$M_4 = a_1 k_1 + a_2 k_2 \tag{A.64}$$

The U_4 displacement is obtained by integrating Eq. A.59 and using the displacement matching boundary condition $U_4(0) = U_1(0)$.

$$U_4 = \frac{1}{A_{11(1)}} \left(\frac{P}{2b} x + \frac{a_1}{s_1} + \frac{a_2}{s_2} \right) + a_3 \tag{A.65}$$

Similarly, integrating Eq. A.64 and setting $\beta_4(a)$ to zero gives the solution for β_4. Using the solutions for Q_4 and β_4 and the boundary condition $W_4(0)=0$ in Eq. A.63 yields the solution for W_4.

In order to determine a_1, a_2 and a_3, the following boundary conditions are used.

$$N_1(0) = \frac{P}{2b}$$

$$\beta_1(0) = \beta_4(0)$$

$$U_1(-L+a) = 0$$

It is convenient to define the following parameters.

$$\theta_1 = \frac{s_1}{A_{55(1)}}\left(k_1 + \frac{h_1}{2}\right) \tag{A.66}$$

$$\theta_2 = \frac{k_1}{D_{11(1)}} \tag{A.67}$$

$$\theta_3 = \frac{s_2}{A_{55(1)}}\left(k_2 + \frac{h_1}{2}\right) \tag{A.68}$$

$$\theta_4 = \frac{k_2}{D_{11(1)}} \tag{A.69}$$

$$\theta_d = \theta_3 - \theta_1 + (\theta_4 - \theta_2)a \tag{A.70}$$

The nominal (far field) strain is given by

$$\varepsilon = \frac{P}{2b}\frac{1}{A_{11(1)} + A_{11(2)}} \tag{A.71}$$

The a parameters are obtained as

$$a_1 = A_{11(2)}\varepsilon\,\frac{\theta_3+\theta_4 a}{\theta_d} \tag{A.72}$$

$$a_2 = -A_{11(2)}\varepsilon\,\frac{\theta_1+\theta_2 a}{\theta_d} \tag{A.73}$$

$$a_3 = \varepsilon\,(L-a) - \frac{a_1}{s_1 A_{11(1)}}\,e^{-s_1(L-a)} - \frac{a_2}{s_2 A_{11(1)}}\,e^{-s_2(L-a)} \tag{A.74}$$

The specimen compliance C is defined as the ratio of specimen extension to applied load. This is obtained as

$$C = \frac{2U_4(a)}{P}$$

$$= \frac{2}{PA_{11(1)}}\left\{\frac{Pa}{2b} + \frac{a_1}{s_1} + \frac{a_2}{s_2} + a_3A_{11(1)}\right\} \qquad (A.75)$$

The total energy release rate associated with the crack (delamination) growth under a constant load P is given by

$$G_T = \frac{P^2}{2b}\frac{dC}{da} \qquad (A.76)$$

Substituting the compliance expression from Eq. A.75 in Eq. A.76 yields the following expression for the total energy release rate.

$$G_T = \frac{P^2}{2b^2}\left(\frac{1}{A_{11(1)}} - \frac{1}{A_{11(1)}+A_{11(2)}} + I_1 - I_2\right) \qquad (A.77)$$

where

$$I_1 = \chi\,\frac{\theta_2\theta_3-\theta_1\theta_4}{\theta_d^2}\left(\frac{1-e^{-s_1(L-a)}}{s_1} - \frac{1-e^{-s_2(L-a)}}{s_2}\right) \qquad (A.78)$$

$$I_2 = \chi\,\frac{(\theta_3+\theta_4 a)e^{-s_1(L-a)} - (\theta_1+\theta_2 a)e^{-s_2(L-a)}}{\theta_d} \qquad (A.79)$$

with

$$\chi = \frac{1}{A_{11(1)}+A_{11(2)}}\frac{A_{11(2)}}{A_{11(1)}} \qquad (A.80)$$

The individual fracture mode contributions to the energy release rate can be calculated using the virtual crack closure method, based on the interlaminar stresses and displacements in the vicinity of the crack tip. From the assumed plane strain condition, the mode III contribution is zero ($G_{III}=0$). The mode II energy release rate, G_{II}, is calculated using the virtual crack closure technique while G_I is evaluated using

$$G_I = G_T - G_{II} \qquad (A.81)$$

G_{II} is calculated from the interlaminar shear stress and relative sliding displacement as

$$G_{II} = \lim_{\delta\to 0}\frac{1}{2\delta}\int_0^{\delta} T_1(x-\delta)\Delta u(x)dx \qquad (A.82)$$

In the absence of a singularity in the stress field, the limiting process leads to the trivial result $G_{II}=0$. Hence, the limit is calculated as δ tends to some finite value, say Δ. The value of Δ is chosen depending on the decay length associated with the problem i.e. the length within which the presence of the crack significantly alters the specimen response in comparison with the corresponding far field values. The decay length in this problem is dependent on the eigenvalues s_1 and s_2. The following value of Δ has been chosen in order to reasonably fulfil the decay length criterion.

$$\Delta = \frac{1}{4}\left(\frac{1}{s_1}+\frac{1}{s_2}\right) \tag{A.83}$$

The relative sliding displacement Δu is based only on the difference U_4-U_3 so that the kinematic condition of zero relative displacement at the crack tip is fulfilled. This also simplifies the calculations. If the true value of Δu (based on u_4-u_3) is used, the β mismatch at the 3-4 interface leads to a kinematically inadmissible displacement discontinuity at the interface. This discontinuity causes a non trivial limiting value G_{II} as $\delta \rightarrow 0$. But this value is an artifact of the modeling assumptions and cannot be used as the true value of G_{II}. The mode II energy release rate component, using $\Delta u = U_4 - U_3$, is obtained as

$$G_{II} = \frac{I_3}{2\Delta} \tag{A.84}$$

where the parameter I_3 depends on $A_{11(1)}$, $A_{11(2)}$, s_1, s_2, a_1, a_2, Δ and the specimen nominal strain ε.

Table I Summary of Results

number of 90° plies	G_T J/m^2	G_{II}/G_T	σ_c MPa	ϵ_c %
1/2	2.404	0.276	1313.9	1.6747
1	6.752	0.275	784.0	1.1685
2	22.849	0.267	426.2	0.8058
3	51.049	0.261	285.1	0.6427
4	93.603	0.256	210.6	0.5444
6	228.871	0.250	134.7	0.4264
8	440.065	0.247	97.1	0.3555

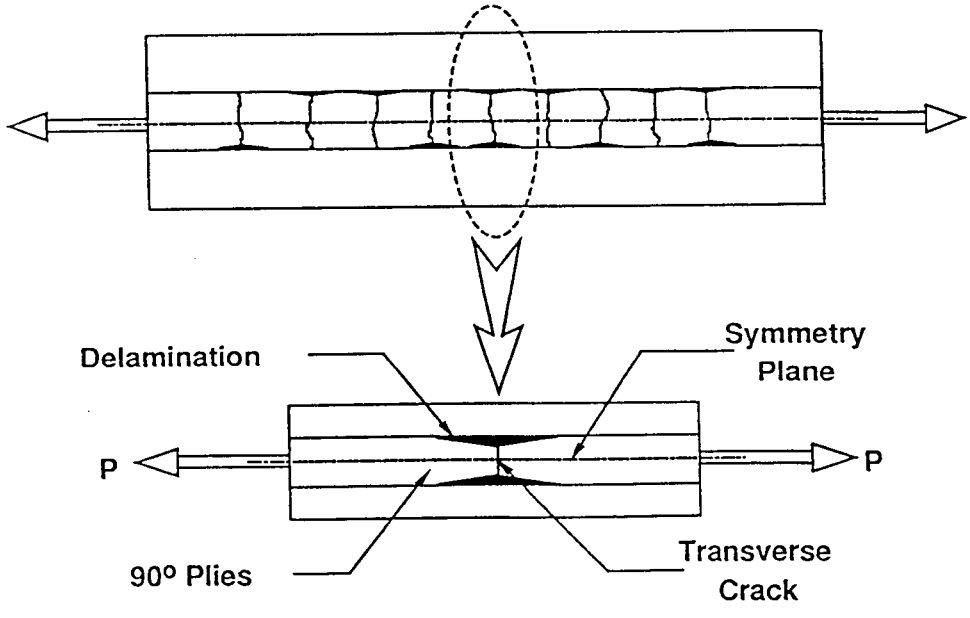

Fig. 1 Specimen Cross Section

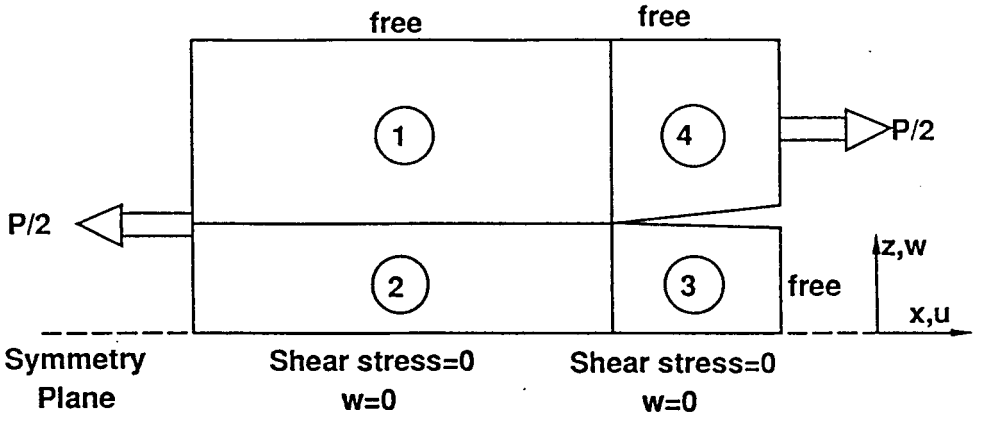

Fig. 2 Modelled Region and Sublaminate Scheme

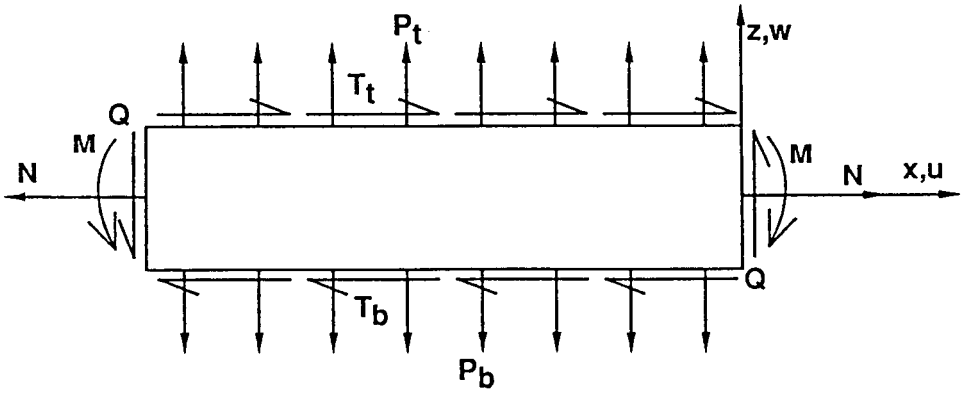

Fig. 3 Generic Sublaminate

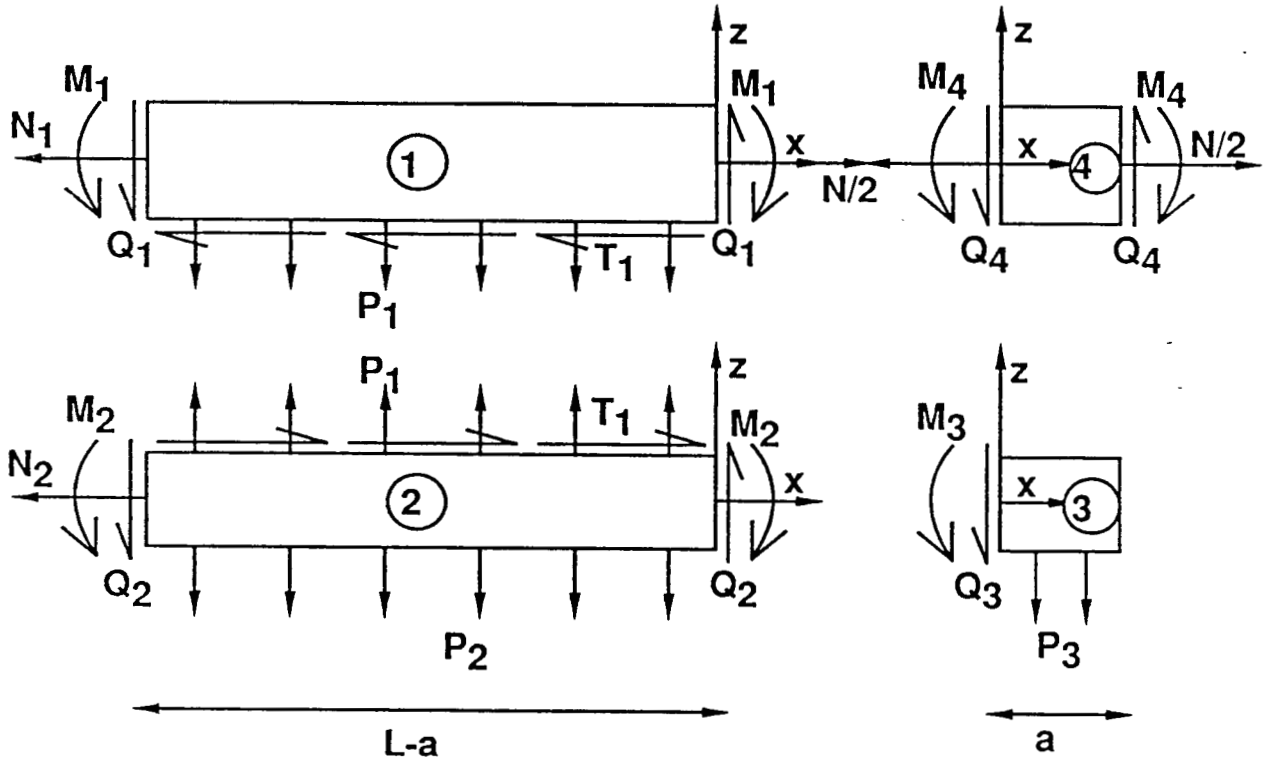

Fig. 4 Sublaminate Forces and Coordinate Systems

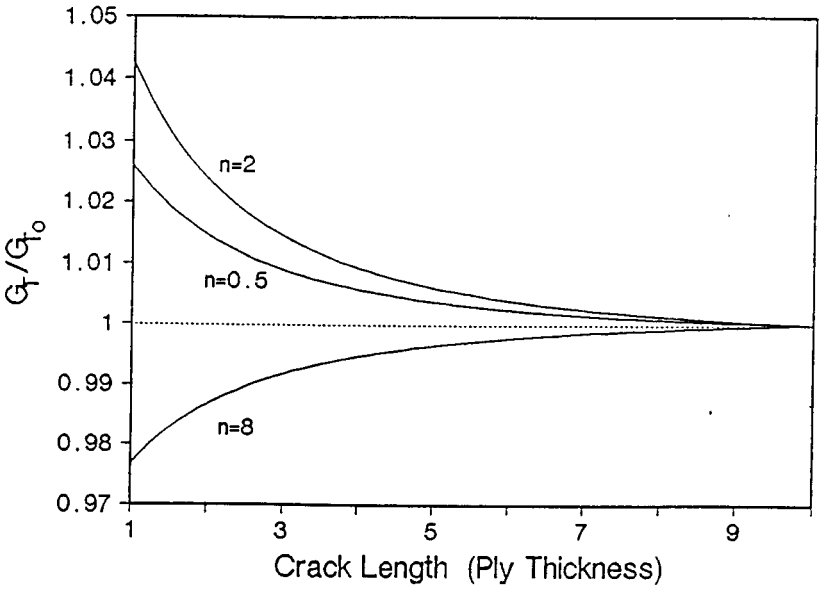

Fig. 5 Total Energy Release Rate Variation with Crack Size

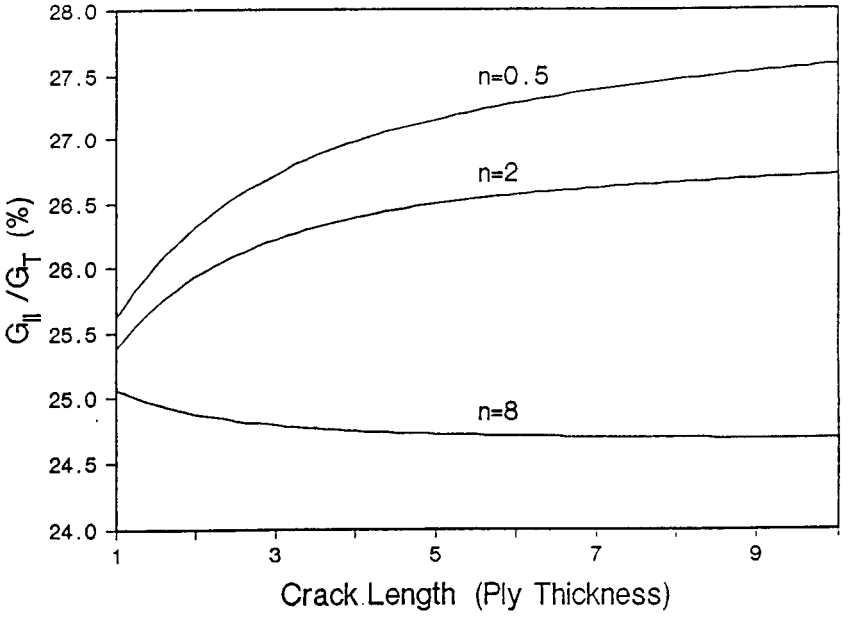

Fig. 6 Mode II Energy Release Rate Dependence on Crack Size

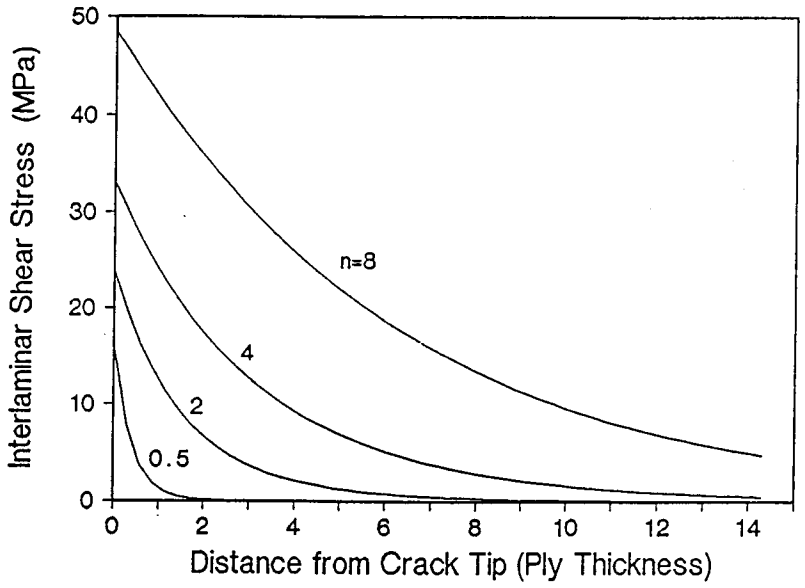

Fig. 7 Interlaminar Shear Stress Distribution

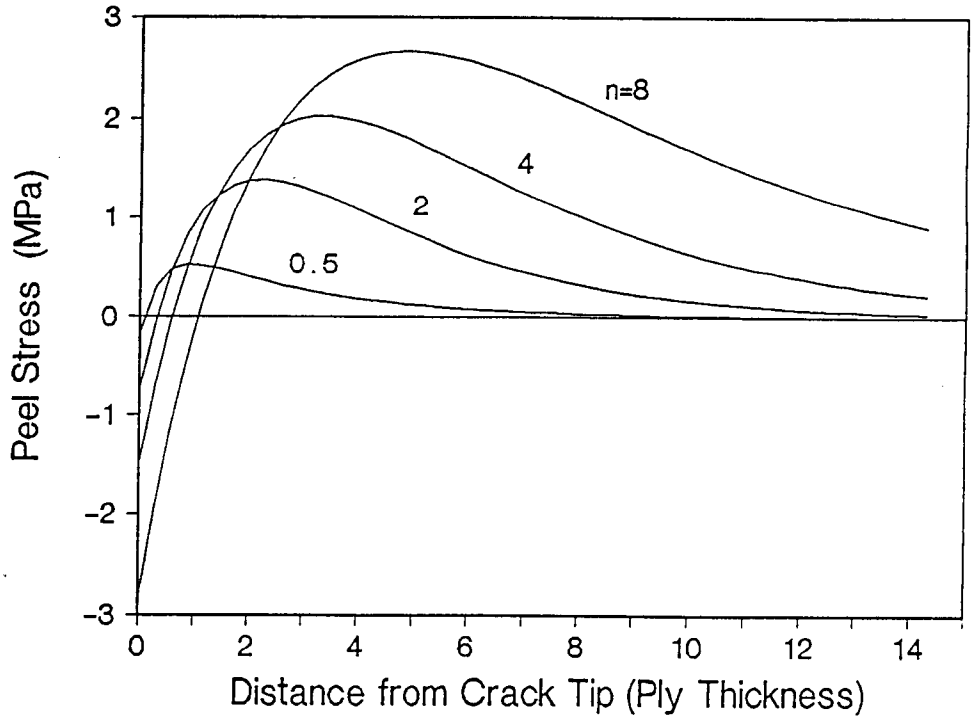

Fig. 8 Interlaminar Normal Stress (Peel Stress) Distribution

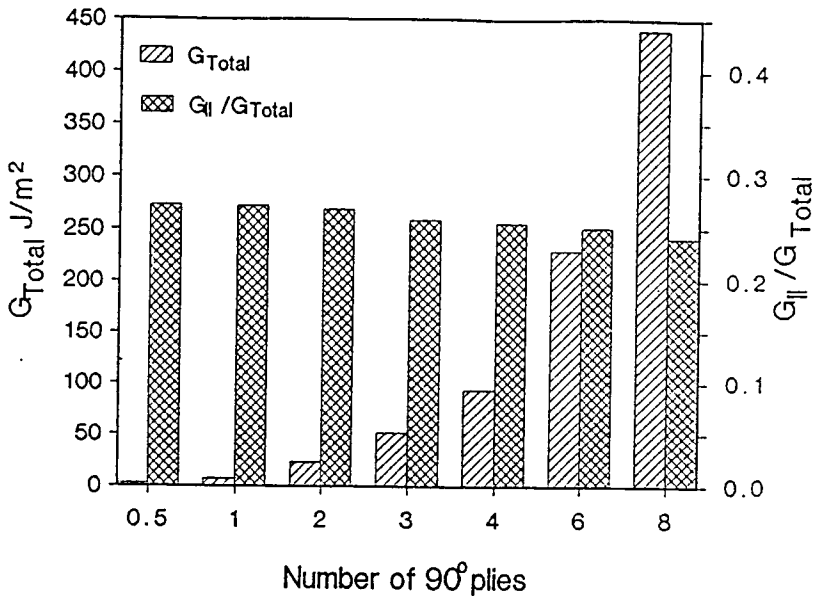

Fig. 9 Energy Release Rate Comparison

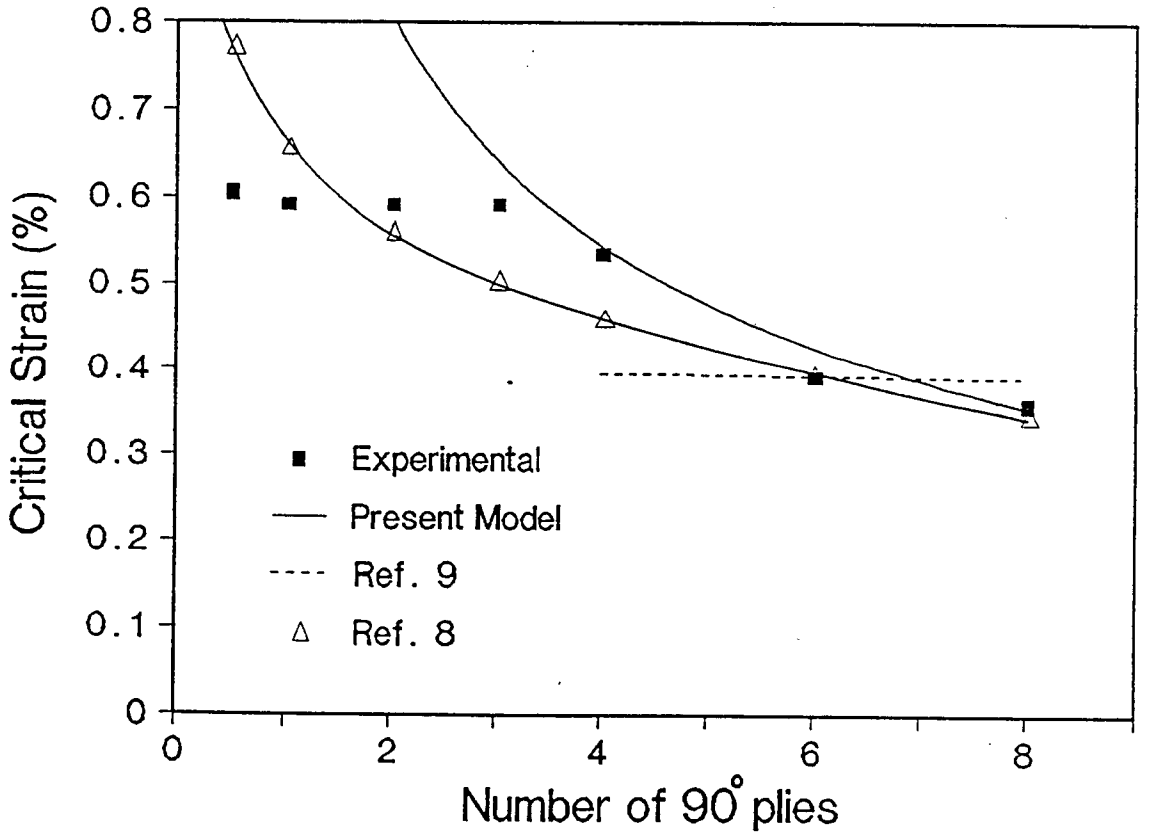

Fig. 10 Critical Delamination Growth Strain Variation